Research Article | Vol. 14, No. 8 / 1 Aug 2024 / Optical Materials Express 2032
Optical Materials EXPRESS

Inverse design of topological photonic time crystals via deep learning

YANG LONG,[1,6] LINYANG ZOU,[2] LETIAN YU,[1] HAO HU,[3] JIANG XIONG,[4] AND BAILE ZHANG[1,5,7]

[1]Division of Physics and Applied Physics, School of Physical and Mathematical Sciences, Nanyang Technological University, 21 Nanyang Link, Singapore 637371, Singapore
[2]School of Electrical and Electronic Engineering, Nanyang Technological University, Singapore, 639798, Singapore
[3]National Key Laboratory of Microwave Photonics, Nanjing University of Aeronautics and Astronautics, Nanjing, China
[4]School of Physics, University of Electronic Science and Technology of China, Chengdu 610054, China
[5]Centre for Disruptive Photonic Technologies, Nanyang Technological University, Singapore 637371, Singapore
[6]yang.long.physics@outlook.com
[7]blzhang@ntu.edu.sg

Abstract: Photonic time crystals are a new kind of photonic system in modern optical physics, leading to devices with new properties in time. However, so far, it is still a challenge to design photonic time crystals with specific topological states due to the complex relations between time crystal structures and topological properties. Here, we propose a deep-learning-based approach to address this challenge. In a photonic time crystal with time inversion symmetry, each band separated by momentum gaps can have a non-zero quantized Berry phase. We show that the neural network can learn the relationship between time crystal structures and Berry phases, and then determine the crystal structures of photonic time crystals based on given Berry phase properties. Our work shows a new way of applying machine learning to the inverse design of time-varying optical systems and has potential extensions to other fields, such as time-varying phononic devices.

Photonic time crystals (PTCs) are a new form of photonic crystal with dielectric properties that vary periodically over time [1–6]. Recent research has shown that PTCs can exhibit topological phases, where bands separated by momentum gaps possess a non-zero Berry phase determined by Bloch boundary conditions in time [7]. Differences in Berry phases between two PTCs can result in the emergence of topological edge states, enabling the design of robust optical devices in time. However, the relationship between the topological properties and time crystal structure of the PTC is complex and not easily captured by a simple formula, highlighting the need for an efficient method to design PTCs with desired topological properties.

Machine learning has widely demonstrated the effectiveness in exploring expert-level game play and optimizing complex strategies [8,9], as seen in mastering the game of Go [10–12], detecting critical diseases [13], and controlling advanced robots automatically [14,15]. Recently, machine learning has been applied to explore quantum states [16,17], design optical structures inversely [18–23], and identify the topological phase [24–27]. Thus, machine learning can become an efficient approach for realizing inverse design of PTCs with the target topological properties.

In this work, we exploit deep learning to realize the efficient inverse design of the topological PTCs with the target topological properties. Our approach involves describing the structures and the topological properties of PTCs, exploiting a pre-trained tandem pipeline to realize an inverse design model, and generating the time crystal structure of PTCs with the target

#525396 https://doi.org/10.1364/OME.525396
Journal © 2024 Received 2 Apr 2024; revised 26 Jun 2024; accepted 8 Jul 2024; published 23 Jul 2024

Optical Materials EXPRESS

topological properties. Our work shows a new way about the applicability of machine learning in designing complex optical functions, including topological properties, and demonstrates potential extensions to the design of time-varying devices in other classical wave systems, e.g., phononic devices.

A PTC can be represented by a periodic function of optical parameters, e.g., a periodic square-wave-like form in Fig. 1(a). When the medium undergoes a sudden change in optical parameters, a propagating wave in it can exhibit time reflection and refraction. The periodic variation in optical parameters leads to interference between time-reflected and time-refracted waves, creating bands and gaps in momentum space [28]. Modes within momentum gaps can undergo exponential amplification over time, offering a new approach for radiation amplification or lasing [1]. PTCs exhibit two important features [4]: (1) PTCs break the conservation of energy of the system; (2) PTCs can be spatially homogeneous, meaning that momentum is conserved.

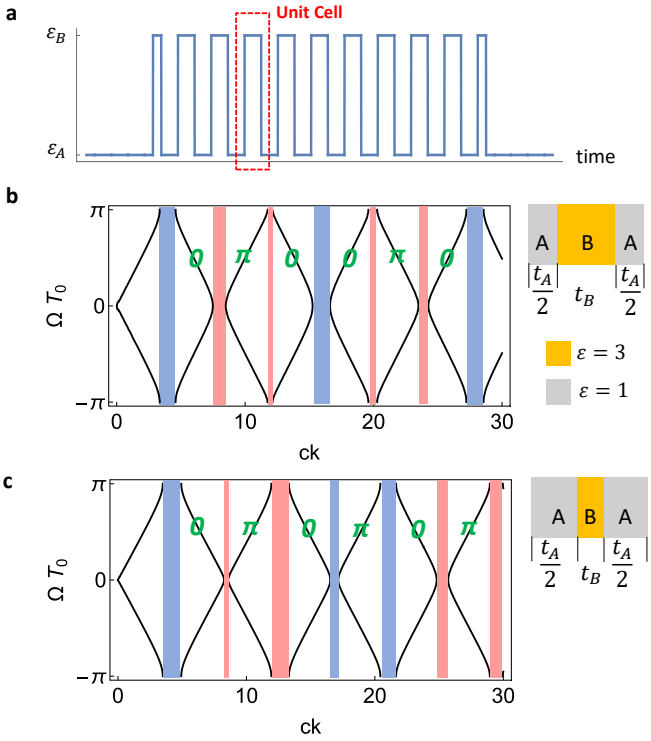

Fig. 1. Momentum-gap topology and its sensitivity to the time crystal structures. (a) PTC can be represented by a function of the relative permittivity in time. In our work, we consider the unit relative permeability, i.e., $\mu = 1$ for simplicity. The red dashed line denotes the unit cell of the PTC. (b) The band structure, topological properties and the sign of the relative phase ϕ of a PTC with the time inversion symmetry. Here, $\varepsilon_A = 3$ and $\varepsilon_B = 1$. Here, $t_A = 0.5$ and $t_B = 0.5$, $T = t_A + t_B$. The Berry phase of each individual band is labeled in green. The red/blue strip represents the gap with the positive/negative relative phase ϕ. (c) The band structure, topological properties and the sign of the relative phase ϕ of a PTC with only the time crystal structure changed. Here, $t_A = 0.4$ and $t_B = 0.6$.

To have the topological properties of the PTC, we need to consider the time inversion symmetry [7], namely $\varepsilon(t) = \varepsilon(-t)$, where ε is the temporal permittivity. Due to the time periodicity $\varepsilon(t) = \varepsilon(t + T)$ where T is the time period, a time Bloch boundary is introduced, namely the wave function will carry a Bloch coefficient $e^{-i\Omega T}$, where $\Omega = \frac{2\pi}{T}$. According to the inversion

Optical Materials EXPRESS

symmetry condition, we can have the quantized Berry phase as the topological invariant [7]:

$$\theta_m = \int_{-\pi/T}^{\pi/T} d\Omega \left(i \int_0^T dt \varepsilon(t) D^*_{m,\Omega}(t) \partial_\Omega D_{m,\Omega}(t) \right) = 0, \pi \tag{1}$$

where m is the band index and $D_{m,\Omega}(t)$ is the Floquet mode of the displacement field. Importantly, the topological properties of PTCs are influenced by the time crystal structure. We calculated the Berry phase for one case, as shown in Fig. 1(b). Altering the time crystal structure results in changes to the Berry phases of the bands, as illustrated in Fig. 1(c), demonstrating that a slight change in parameters can alter the Berry phases of bands. It is also possible for two geometrically different photonic time crystals to have identical topological properties. These facts show that the relationship between Berry phase and time crystal structure is complex and cannot be described by simple mathematical formulas. Furthermore, the quantized nature of topological invariant makes it unsuitable for optimization using conventional gradient-based algorithms. Thus, designing the appropriate time crystal structure to achieve the desired topological properties in the target momentum region is challenging and complicated. In the following sections, we will present a machine-learning approach to design PTCs with specific topological properties.

In our work, we assume two dielectric media: A and B. We set $\varepsilon_A = 1$ and $\varepsilon_B = 3$ for simplicity [7]. We focus on the time crystal structures of PTCs with the time inversion symmetry. So that the unit cell is symmetric with the configuration $(\frac{t_1}{2}, t_2, \ldots, t_M, \ldots, t_2, \frac{t_1}{2})$. As illustrated in Fig. 2(a), we set $M = 4$. We can define a state vector $\boldsymbol{t}_s$ to represent the time duration of each layer in the unit cell, given by $\boldsymbol{t}_s = (t_1, t_2, t_3, t_4)$. For describing the topological properties, as shown in Fig. 2(b), we exploit a $1 \times N$ vector as the label vector $\boldsymbol{\beta}$, which represent sign properties of the relative phases ϕ. For the n-th momentum gap, $\phi_n = \arg\left[\frac{A_r}{A_t}\right]$, where A_r and A_t are the time-reflected and time-refracted coefficient. For the each momentum point k_j, $\beta_j = \text{sign}[\phi(k_j)]$ ($\text{sign}[\phi_n] = -1$ for $\phi_n \in (-\pi, 0)$; otherwise, $\text{sign}[\phi_n] = 1$) for the momentum gap; otherwise, $\beta_j = 0$ for the bulk band. The momentum region of interest $[k_{\min}, k_{\max}]$ is divided into N parts $\{k_j\}, j \in 1 \cdots N$. In our work, we set $N = 100$. Note that we don't exploit Berry phase of bands to represent the topological properties of the PTC. This is because the Berry phases of each band can be linked to the relative phase ϕ_n within the momentum gap [7]:

$$\text{sign}[\phi_{n-1}]/\text{sign}[\phi_n] = -e^{i\theta_n}, \quad \theta_n = 0, \pi. \tag{2}$$

As shown in Fig. 3(a), for achieving the forward prediction and inverse design, we introduce the following two neural networks: the forward prediction network $\mathcal{F}$ and the inverse design network $\mathcal{G}$:

$$\boldsymbol{\beta} = \mathcal{F}(\boldsymbol{t}_s), \quad \boldsymbol{t}_s = \mathcal{G}(\boldsymbol{\beta}). \tag{3}$$

The main goal of our work is to obtain $\mathcal{G}$. However, the training will converge slow or finally diverge, if we train the inverse network $\mathcal{G}$ by directly using the dataset $\{\boldsymbol{t}_{s,i}, \boldsymbol{\beta}_i\}$, as the topological properties are not uniquely locking to a PTC, namely, one-to-many question [23,29]. To overcome the one-to-many issue, we exploit the solution introduced in Ref. [23], namely, training a tandem network consisting of $\mathcal{G}$ followed by a pre-trained $\mathcal{F}$, rather than training $\mathcal{G}$ solely, as shown in Fig. 3(b). According to Fig. 3(b), the training process of $\mathcal{G}$ can be understood as training an autoencoder. The label vector is encoded by $\mathcal{G}$ into a state vector, and then the information in the state vector is decoded back into the "original" label vector by $\mathcal{F}$. This training approach will make that $\mathcal{G}$ produces an identical state vector if the input label vector remains the same, while addressing the divergence caused by the one-to-many problem.

The details about the network $\mathcal{F}$ and $\mathcal{G}$ are shown below. We train the forward network with the dataset $\{\boldsymbol{t}_{s,i}, \boldsymbol{\beta}_i\}$, while train the tandem network with the dataset $\{\boldsymbol{\beta}_i, \boldsymbol{\beta}_i\}$. The training

Optical Materials EXPRESS

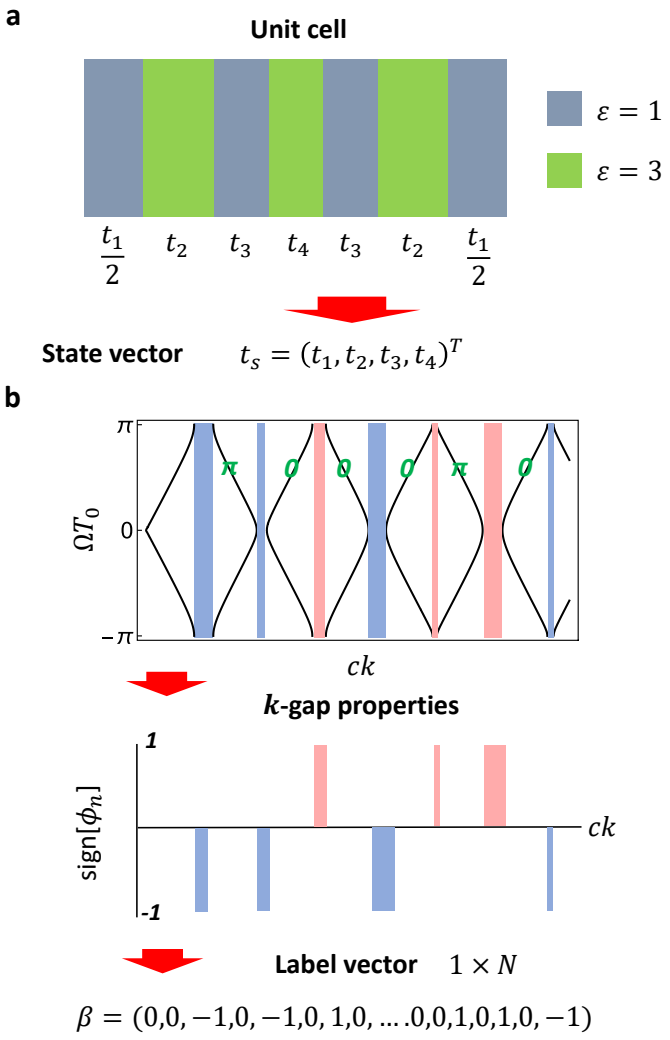

Fig. 2. The state vector and the label vector for a PTC. (a) The state vector constructed by the time duration of each layer in the unit cell. (b) The label vector composed of the sign of the relative phases of momentum gaps. The colorful strips denote the signs of the relative phases: red for ϕ>0 and blue for ϕ<0. Both the band structure characteristics and the system's topological properties can be described in the vector $\boldsymbol{\beta}$.

Optical Materials EXPRESS

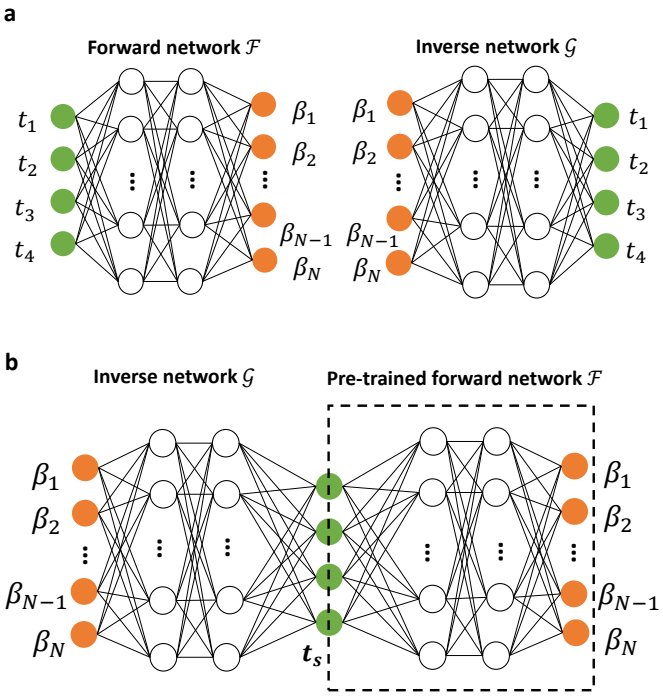

Fig. 3. The forward/inverse network and the schematic representation of training the inverse network. (a) The forward network $\mathcal{F}$ and the inverse network $\mathcal{G}$. (b) A tandem network is composed of $\mathcal{G}$ connected to a pre-trained $\mathcal{F}$. For training the tandem network, we only update the weights in $\mathcal{G}$, but we fix all the weights in the pre-trained $\mathcal{F}$.

process for $\mathcal{F}$ in Fig. 3(a) is to minimize the loss between the state vectors and the label ones:

$$\min_{\mathcal{F}} \frac{1}{N_s} \sum_{i=1}^{N_s} ||\mathcal{F}(\boldsymbol{t}_{s,i}) - \boldsymbol{\beta}_i||^2 + \epsilon ||w_{\mathcal{F}}||_2^2 \tag{4}$$

where N_s is the batch size and $w_{\mathcal{F}}$ represents all the weights and biases in $\mathcal{F}$ (namely, the second term is a $\mathbb{L}_2$ norm). The layer structures of $\mathcal{F}$ are: $(100, 512, 512, 512, 512, 512, 512, 4)$. The activation function for all layers is Tanh function. We train $\mathcal{F}$ with the 5×10^5 random samples (90% for the train set and 10% for the test set). The optimizer for training $\mathcal{F}$ is the Adam optimizer with a learning rate of 0.001. The training process for $\mathcal{G}$ (i.e., the tandem network in Fig. 3(b)) is to minimize the loss between the label vectors and the predicted ones:

$$\min_{\mathcal{G}} \frac{1}{N_s} \sum_{i=1}^{N_s} ||\mathcal{F}(\mathcal{G}(\boldsymbol{\beta}_i)) - \boldsymbol{\beta}_i||^2 + \epsilon ||w_{\mathcal{G}}||_2^2 \tag{5}$$

where N_s is the batch size and $w_{\mathcal{G}}$ represents all the weights and biases in $\mathcal{G}$ (namely, the second term is a $\mathbb{L}_2$ norm). . The layer structures of $\mathcal{G}$ are: $(4, 1024, 1024, 1024, 1024, 1024, 1024, 100)$. The activation function is ReLU function except the final layer; Sigmoid function for the final layer. The optimizer for training $\mathcal{G}$ is the Adam optimizer with a learning rate of 0.001. We set $\epsilon = 10^{-5}$ in the $\mathbb{L}_2$ norm term in $\mathcal{F}$ and $\mathcal{G}$. The number of the training epoch is 5000 and the batch size is $N_s = 2000$.

Here, we demonstrate some examples of inversely designing PTCs with specific target topological properties. The momentum region is set as $ck \in [0, 5]$. As shown in Fig. 2(a), we

Optical Materials EXPRESS

consider a PTC constructed from a unit cell of 7 layers, exhibiting time inversion symmetry. Thereby, we can describe it using the state vector $\boldsymbol{t}_s = (t_1, t_2, t_3, t_4)^T$. We obtain $\mathcal{G}$ by the approach illustrated in Fig. 3(b). As shown in Fig. 4, we demonstrate two cases, for simplicity. The Berry phase θ_n for the n-th band can be controlled by the label vectors of momentum gaps on the both sides of the n-th band. The first case in Fig. 4(a) realizes that all bands are trivial (zero Berry phase). The second case in Fig. 4(d) has non-zero Berry phase for the second band. The target label vectors are represented by the blue line, and the label vectors of the generated PTC by $\mathcal{G}$ are shown as the red point. From these results, we can see that $\mathcal{G}$ is capable of generating the time crystal structures to have the target topological properties. In Figs 4(b,e), we further verifies the Berry phase properties of these generated PTCs by calculating the relative phase ϕ. The band dispersions of these generated PTCs are shown in Figs 4(c,f), with the Berry phase of each band denoted in green.

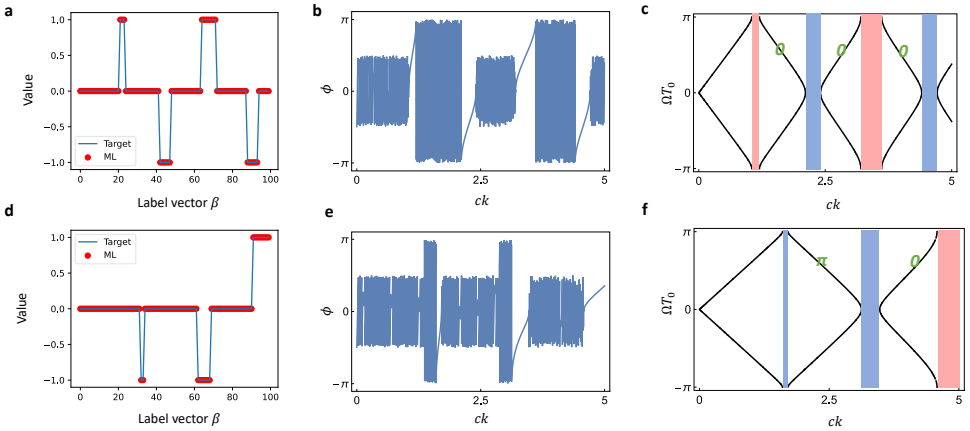

Fig. 4. PTCs designed by $\mathcal{G}$. Two cases are shown in (a) and (d), respectively. The target label vectors are shown in blue, while the label vectors of the optical structures obtained by $\mathcal{G}$ are shown in red. The time length of each layer in the unit cell is (a) $\boldsymbol{t}_s = (0.667, 0.034, 0.834, 0.655)$; (d) $\boldsymbol{t}_s = (0.246, 0.290, 0.561, 0.246)$. (b,e) The corresponding relative phase ϕ spectra. (c,f) The band dispersion (black line) of these PTCs in (a,d). The Berry phase of each band is labeled in green. The colorful strips denote the signs of the reflection phases: red for ϕ>0 and blue for ϕ<0.

To summarize, we show a machine learning-based method for inversely designing PTCs with specific topological properties. To overcome the non-uniqueness problem, we train the inverse network by a tandem pipeline like the autoenconder. In addition to topological properties, our approach can be applied to the inverse design of other optical systems. For instance, we can first train a forward network to learn the relationship between the geometrical parameters and the optical behavior (e.g., transmission, reflection, absorption spectra) of a metasurface according to the optimization task. By forming a tandem network with the pre-trained forward network, we can then obtain an inverse network capable of generating the target structure. Our approach offers new insights into designing topological time-varying optical materials [30–33] and it has potential applications in exploring topological properties in other systems [34,35], e.g., phononics [36,37] and diffusion systems [38,39].

Funding. National Research Foundation Singapore (Competitive Research Program NRF-CRP23-2019-0007); Ministry of Education - Singapore Academic Research Fund Tier 2 (MOE-T2EP50123-0007); Distinguished Professor Fund of Jiangsu Province (1004-YQR23064); Selected Chinese Government Talent-recruitment Programs of Nanjing (1004-YQR23122); the Eric and Wendy Schmidt AI in Science Postdoctoral Fellowship.

Disclosures. The authors declare no conflicts of interest.

Optical Materials EXPRESS

Data availability. Data underlying the results presented in this paper are not publicly available at this time but may be obtained from the authors upon reasonable request.

References

1. M. Lyubarov, Y. Lumer, A. Dikopoltsev, *et al.*, "Amplified emission and lasing in photonic time crystals," Science **377**(6604), 425–428 (2022).
2. Y. Sharabi, E. Lustig, and M. Segev, "Disordered photonic time crystals," Phys. Rev. Lett. **126**(16), 163902 (2021).
3. T. Liu, J.-Y. Ou, K. F. MacDonald, *et al.*, "Photonic metamaterial analogue of a continuous time crystal," Nat. Phys. **19**(7), 986–991 (2023).
4. E. Galiffi, R. Tirole, S. Yin, *et al.*, "Photonics of time-varying media," Adv. Photon. **4**(01), 1 (2022).
5. X. Wang, M. S. Mirmoosa, V. S. Asadchy, *et al.*, "Metasurface-based realization of photonic time crystals," Science Advances **9**, 1 (2023).
6. S. Sadhukhan and S. Ghosh, "Defect in photonic time crystals," Phys. Rev. A **108**(2), 023511 (2023).
7. E. Lustig, Y. Sharabi, and M. Segev, "Topological aspects of photonic time crystals," Optica **5**(11), 1390 (2018).
8. Y. LeCun, Y. Bengio, and G. Hinton, "Deep learning," Nature **521**(7553), 436–444 (2015).
9. Z. Ghahramani, "Probabilistic machine learning and artificial intelligence," Nature **521**(7553), 452–459 (2015).
10. D. Silver, A. Huang, C. J. Maddison, *et al.*, "Mastering the game of go with deep neural networks and tree search," Nature **529**(7587), 484–489 (2016).
11. D. Silver, J. Schrittwieser, K. Simonyan, *et al.*, "Mastering the game of go without human knowledge," Nature **550**(7676), 354–359 (2017).
12. J. Schrittwieser, I. Antonoglou, T. Hubert, *et al.*, "Mastering atari, go, chess and shogi by planning with a learned model," Nature **588**(7839), 604–609 (2020).
13. Y. Liu, A. Jain, C. Eng, *et al.*, "A deep learning system for differential diagnosis of skin diseases," Nat. Med. **26**(6), 900–908 (2020).
14. X. Yin and R. Müller, "Integration of deep learning and soft robotics for a biomimetic approach to nonlinear sensing," Nat Mach Intell **3**(6), 507–512 (2021).
15. A. I. Chen, M. L. Balter, T. J. Maguire, *et al.*, "Deep learning robotic guidance for autonomous vascular access," Nat Mach Intell **2**(2), 104–115 (2020).
16. G. Carleo and M. Troyer, "Solving the quantum many-body problem with artificial neural networks," Science **355**(6325), 602–606 (2017).
17. L. Lewis, H.-Y. Huang, V. T. Tran, *et al.*, "Improved machine learning algorithm for predicting ground state properties," Nat. Commun. **15**(1), 895 (2024).
18. Z. Liu, D. Zhu, L. Raju, *et al.*, "Tackling photonic inverse design with machine learning," Adv. Sci. **8**, 1 (2021).
19. N. Wang, W. Yan, Y. Qu, *et al.*, "Intelligent designs in nanophotonics: from optimization towards inverse creation," PhotoniX **2**(1), 22 (2021).
20. Y. Chen, Z. Lan, Z. Su, *et al.*, "Inverse design of photonic and phononic topological insulators: a review," Nanophotonics **11**(19), 4347–4362 (2022).
21. S. So, T. Badloe, J. Noh, *et al.*, "Deep learning enabled inverse design in nanophotonics," Nanophotonics **9**(5), 1041–1057 (2020).
22. P. R. Wiecha, A. Arbouet, C. Girard, *et al.*, "Deep learning in nano-photonics: inverse design and beyond," Photonics Res. **9**(5), B182 (2021).
23. Y. Long, J. Ren, Y. Li, *et al.*, "Inverse design of photonic topological state via machine learning," Appl. Phys. Lett. **114**(18), 181105 (2019).
24. J. F. Rodriguez-Nieva and M. S. Scheurer, "Identifying topological order through unsupervised machine learning," Nat. Phys. **15**(8), 790–795 (2019).
25. M. S. Scheurer and R.-J. Slager, "Unsupervised machine learning and band topology," Phys. Rev. Lett. **124**(22), 226401 (2020).
26. Y. Long, J. Ren, and H. Chen, "Unsupervised manifold clustering of topological phononics," Phys. Rev. Lett. **124**(18), 185501 (2020).
27. Y. Long and B. Zhang, "Unsupervised data-driven classification of topological gapped systems with symmetries," Phys. Rev. Lett. **130**(3), 036601 (2023).
28. J. R. Reyes-Ayona and P. Halevi, "Observation of genuine wave vector (k or β) gap in a dynamic transmission line and temporal photonic crystals," Applied Physics Letters **107**(7), 1 (2015).
29. D. Liu, Y. Tan, E. Khoram, *et al.*, "Training deep neural networks for the inverse design of nanophotonic structures," ACS Photonics **5**(4), 1365–1369 (2018).
30. A. Dikopoltsev, Y. Sharabi, M. Lyubarov, *et al.*, "Light emission by free electrons in photonic time-crystals," Proc. Natl. Acad. Sci. U.S.A. **119**(6), 1 (2022).
31. H. Li, S. Yin, H. He, *et al.*, "Stationary charge radiation in anisotropic photonic time crystals," Phys. Rev. Lett. **130**(9), 093803 (2023).
32. Y. Yu, H. Hu, L. Zou, *et al.*, "Antireflection spatiotemporal metamaterials," Laser & Photonics Reviews **17**, 1 (2023).
33. Q. Yang, H. Hu, X. Li, *et al.*, "Cascaded parametric amplification based on spatiotemporal modulations," Photonics Res. **11**(5), B125 (2023).
34. Y. Peng, "Topological space-time crystal," Phys. Rev. Lett. **128**(18), 186802 (2022).

Optical Materials EXPRESS

35. S. Xu and C. Wu, "Space-time crystal and space-time group," Phys. Rev. Lett. **120**(9), 096401 (2018).
36. Q. Wu, H. Chen, H. Nassar, *et al.*, "Non-reciprocal Rayleigh wave propagation in space-time modulated surface," J. Mech. Phys. Solids **146**, 104196 (2021).
37. Y. Long, J. Ren, and H. Chen, "Intrinsic spin of elastic waves," Proc. Natl. Acad. Sci. U.S.A. **115**(40), 9951–9955 (2018).
38. H. Hu, S. Han, Y. Yang, *et al.*, "Observation of topological edge states in thermal diffusion," Adv. Mater. **34**, 1 (2022).
39. H. Wu, H. Hu, X. Wang, *et al.*, "Higher-order topological states in thermal diffusion," Adv. Mater. **35**, 1 (2023).